

Use of an experimentally derived leadfield in the peripheral nerve pathway discrimination problem

José Zariffa, *Member, IEEE*, Mary K. Nagai, Martin Schuettler, *Member, IEEE*, Thomas Stieglitz, *Member, IEEE*, Zafiris J. Daskalakis and Milos R. Popovic, *Senior Member, IEEE*

Abstract—The task of discriminating the neural pathways responsible for the activity recorded using a multi-contact nerve cuff electrode has recently been approached as an inverse problem of source localization, similar to EEG source localization. A major drawback of this method is that it requires a model of the nerve, and that the localization performance is highly dependent on the accuracy of this model. Using recordings from a 56-contact “matrix” cuff electrode placed on a rat sciatic nerve, we investigated a method that eliminates the need for a model, and uses instead an “experimental” leadfield constructed from a training set of experimental recordings. The resulting pathway-identification task is solved using an inverse problem framework. The experimental leadfield approach was able to identify the correct branch in cases in which a single fascicle was active with a success rate of 94.2%, but was not able to reliably identify combinations of fascicles. Nevertheless, the proposed methodology provides a framework for the study of multi-pathway discrimination, within which methods to improve performance can be investigated. Specifically, the influence of nerve anatomy and electrode design should be examined, and regularization approaches better suited to this novel inverse problem should be sought.

Index Terms—Pathway discrimination, experimental leadfield, multi-contact cuff electrode, nerve cuff selectivity, peripheral nerve interface, rat sciatic nerve.

I. INTRODUCTION

A Neuroprosthesis is a system in which an artificial device interacts directly with the nervous system in order to replace or enhance damaged function. Our focus here is on implantable neuroprostheses that interact with the peripheral nervous system: these systems can be used to help restore function in subjects with spinal cord injuries, strokes, and amputations. One current limitation of this type of technology is that there is a need for more selective neural interfaces capable of discriminating the electrical activity of different

pathways within a nerve, and therefore allowing more sophisticated control of the neuroprosthesis. For example, by monitoring specific pathways, sensory activity corresponding to a particular location could be decoded and used as part of closed-loop control algorithms for functional electrical stimulation (FES) systems aiming to restore movement in individuals with spinal cord injury or stroke (e.g. [1]–[3]). Alternatively, in the case of amputations, efferent commands to specific muscles could be extracted proximally to the injury and used to control a prosthetic limb [4], [5].

A number of different peripheral nerve interfaces have been proposed. Longitudinally implanted intrafascicular electrodes (LIFE) [6], [7] have very high spatial resolution, but are not able to provide coverage of the whole nerve. Intraneural recordings obtained using micro-electrode arrays (MEA) [8] combine spatially specific recordings with good coverage of the nerve, and so are a potentially attractive option, but have several drawbacks. MEAs may cause damage during chronic implantation, are difficult to use for small nerves (due to manufacturing considerations), and the recording stability over time is poor [9]. Selective recording has also been attempted with nerve cuff electrodes, using methods based either on conduction velocity [10]–[12], or on the spatial variations in the extraneural fields [13]–[20]. This second category of methods either proposed approaches that were not easily generalizable beyond two fascicles, or quantified the selectivity of the cuff without proposing an approach to identify multiple sources from the recordings. Nonetheless, the novel manufacturing methods and nerve cuff designs of recent years [17], [21] have resulted in nerve cuffs that provide greater amounts of information, and have opened the door to new processing approaches.

In order to generalize previous nerve cuff-based approaches to selective recording and best take advantage of multi-contact electrode designs, we have recently explored the idea of using a source localization approach adapted from the field of EEG source localization [22], [23]. Simulations and initial experiments have indicated that in a 1 mm nerve surrounded by a “matrix” design multi-contact spiral nerve cuff [24], one of the crucial conditions for performance to be acceptable is to have an accurate model of the nerve [23], [25]. The importance of the model stems from the fact that the source configuration can only be accurately reconstructed if we have a reasonably good estimate of how a source at a given location would affect the measurements.

Wodlinger et al. have explored a related approach and shown recently that, in the case of a flat interface nerve

Manuscript received August 12, 2010; revised October 14, 2010. This work was supported by the Natural Sciences and Engineering Research Council of Canada (grant #249669), the Ontario Graduate Scholarship program and the Walter C. Sumner Foundation.

J. Zariffa, M.K. Nagai and M.R. Popovic are with the Institute of Biomaterials and Biomedical Engineering, University of Toronto, and the Toronto Rehabilitation Institute, Toronto, Canada. J. Zariffa and M.R. Popovic are also with the Edward S. Rogers Sr. Department of Electrical and Computer Engineering, University of Toronto. Z.J. Daskalakis is with the Schizophrenia Program, Department of Psychiatry, Centre for Addiction and Mental Health, Faculty of Medicine, University of Toronto, Canada. M. Schuettler and T. Stieglitz are with the Laboratory for Biomedical Microtechnology, Department of Microsystems Engineering - IMTEK, University of Freiburg, Germany. Email: milos.popovic@utoronto.ca.

Copyright (c) 2010 IEEE. Personal use of this material is permitted. However, permission to use this material for any other purposes must be obtained from the IEEE by sending a request to pubs-permissions@ieee.org.

cuff electrode placed on a large nerve, major fascicles can be successfully identified using a beamforming approach with knowledge only of the electrode geometry [26], [27]. These results are promising and suggest that peripheral nerve source localization approaches are worth pursuing further, however it is unclear what resolution could be achieved *in vivo* without a more accurate model of the nerve's anatomy, or in the case of combinations of several sources. The sensitivity of source localization approaches to model accuracy therefore remains of interest, particularly because current technology does not allow us to obtain an accurate three-dimensional model of a particular nerve *in vivo*.

In the present study, we investigate a method that aims to circumvent these issues by eliminating the dependency on a model. Instead, a training set of data is collected experimentally and then used as the empirical basis for the interpretation of new data, while still remaining within an inverse problem framework similar to that used in source localization. The motivation for using such a framework is that it provides the means to deal both with combinations of multiple sources and with uncertainty in the measurements.

II. METHODS

A. Data collection

1) *Surgical procedure*: Five male Long-Evans rats (old breeders, 640 g to 850 g) (Charles River Laboratories Inc., Wilmington, MA, USA) were used. The rats were acclimatized for one week prior to use in the experiment, with food and water provided *ad libitum* and a 12 hour lights on/off cycle. All animal care and use procedures conformed to those outlined by the Canadian Council on Animal Care (CCAC).

All animals were anesthetized with a single bolus injection of pentobarbital (60 mg/kg, intraperitoneal), and their lower backs and legs shaved and treated with povidone-iodine. When an adequate depth of anesthesia was attained (loss of corneal reflex and loss of sharp pain sensation), the animals were positioned prone on the operating table.

An oblique incision was centered over the posterior (dorsal) aspect of the hip. The incision was extended proximally to the midline and distally parallel with the fibers of the gluteus maximus to the posterior margin of the greater trochanter. The incision was then directed distally, parallel with the femoral shaft to the posterior fossa of the knee. The deep fascia was exposed and divided in line with the skin incision. By blunt dissection, the gluteus maximus was split in line with its fibers and retracted to expose the sciatic nerve and short external rotator muscles. Care was taken not to disturb the superior gluteal vessels in the proximal part of the exposure.

The sciatic nerve was exposed as far proximally as possible to allow adequate exposure for application of the recording cuff. The sciatic nerve was then followed distally and three branches were identified: the sural nerve, peroneal nerve, and tibial nerve. The soft tissue surrounding each of these nerves was carefully bluntly dissected to allow a stimulating cuff to be applied to each nerve. The three stimulating cuffs were applied first, followed by the recording cuff on the sciatic nerve (see details in the next section).

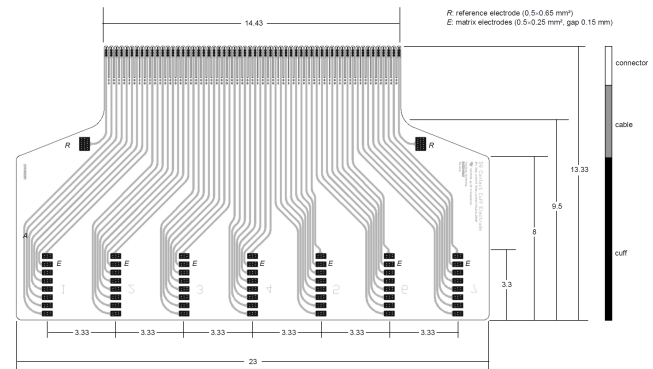
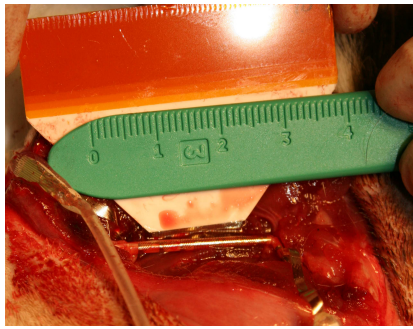


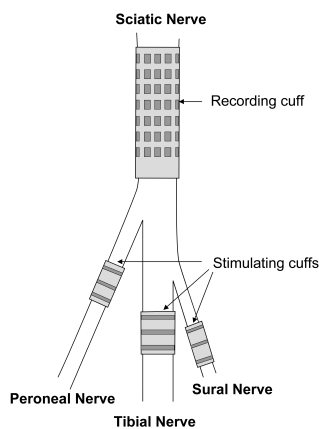
Fig. 1. Planar schematic of the matrix nerve cuff, 1 mm in diameter when rolled. All dimensions are in millimeters.

2) *Recording methods*: A “matrix” design polyimide spiral nerve cuff electrode [24] was used to record the nerve activity during the experiments. The matrix cuff was 23 mm long, 1 mm in diameter and contained 7 rings of 8 contacts, for a total of 56 contacts. The cuff, a diagram of which is shown in Figure 1, was manufactured by placing a 300 nm platinum film between two layers of Pyralin 2611 polyimide. The resulting planar electrode was curled and placed in an aluminum block, then tempered so as to remove mechanical stress and ensure that the structure maintains a curled shape at room temperature. Lastly, the electrode contacts were coated with platinum black. The interconnection technology for the device is described in [28]. The cuff was placed on the sciatic nerve, just proximal to its division into its peroneal and tibial branches (Figure 2(a)). In order to stimulate the nerve branches, three tripolar polyimide spiral nerve cuffs (8 mm long and 1 mm in diameter) were placed around the tibial, sural, and common peroneal nerves. The center ring of the stimulating electrodes contained 8 contacts that were shorted together to create traditional tripole cuffs. A schematic of the cuff placements is shown in Figure 2(b). The rat sciatic nerve is known to branch progressively into four fascicles, which then become the tibial, peroneal, and sural nerves and the much smaller cutaneous branch (not used here) [29]. This branching pattern was verified by histological analysis (hematoxylin and eosin staining at 5 mm intervals along the length of the recording cuff). Therefore, by stimulating the tibial, peroneal, and sural nerves distally, we can control which of the fascicles is active at the level of the recording cuff. This one-to-one correspondence between fascicles and distal nerves does not always hold in the general case, but is valid for the purpose of this study.

The measurements from the recording cuff were acquired using a SynAmps2 64-channel amplifier (Neuroscan Inc., Herndon, VA, USA), with a sampling rate of 20 kHz and a gain of 2010. The signals were band-pass filtered between 300 Hz and 3 kHz. The reference for the recordings was a contact included in the matrix cuff design and located just outside the cuff (Figure 1). A needle electrode in the calf was used as the ground.



(a)



(b)

Fig. 2. (a) 56-contact nerve cuff placed on the sciatic nerve, just proximally to the branching into the tibial and peroneal nerves. (b) Schematic representation of the position of the stimulating and recording nerve cuffs (not exactly to scale)

The tibial, peroneal, and sural nerves were stimulated first individually, then in every possible combination. The stimulation pulses were generated using Compex Motion stimulators (Compex SA, Switzerland), and had estimated durations of 2-4 μ s and amplitudes in the 0.7 to 3.8 mA range approximately (see Discussion section). These pulses were able to reliably produce action potentials in the nerve, as indicated by muscle twitches. 100 trials were conducted for each fascicle, at a frequency of 2 Hz. A stimulation artefact was present because the amplifiers were not blanked during the stimulation due to equipment restrictions. The stimulation pulses did not overlap with the neural signal, and the amplifiers did not saturate, but they were susceptible to an impulse artefact with a time constant of approximately 0.5 ms and thus overlapping with the signal of interest. To compensate for this, the measurements were converted to a common-average reference: the time series from all channels were averaged together, and the resulting average was subtracted from each of the time series, thereby helping to eliminate elements that were common to all signals (Figure 3).

3) *Inverse problem and construction of the leadfield:* Bioelectric source localization is an inverse problem in which

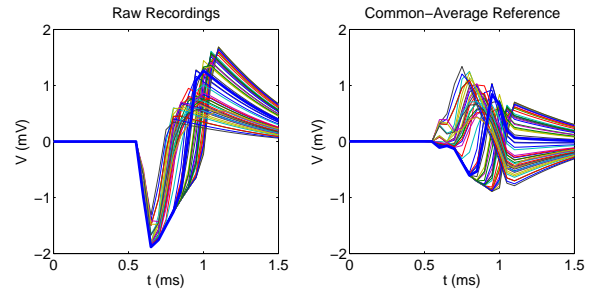


Fig. 3. Recordings of all 56 contacts for one trial in Rat 1, while the tibial branch is being stimulated. The left plot show the raw data, recorded using a point outside the cuff as the reference (see text). The right plot shows the same data after conversion to a common average reference. The lines in bold in both plots correspond to the recordings for one contact in the middle ring of the cuff, and illustrate the reduction of the stimulation artefact.

the bioelectric activity within a region (e.g. head, torso, or nerve) is estimated using measurements obtained on the boundary of that region. Solving the inverse problem requires a solution to the forward problem, which predicts how a source at any given location will affect the measurements at the boundary. This information is encoded in a matrix known as the leadfield. The relationship between the bioelectric sources and the measurements can be expressed as shown in Equation 1, where \mathbf{d} is an $M \times 1$ vector containing the recorded data from the M electrodes contacts, \mathbf{j} is an $N \times 1$ vector whose entries represent the magnitudes of the current dipoles distributed throughout the region under consideration, and \mathbf{L} is the $M \times N$ leadfield matrix whose entry (i,j) represents the influence of a unit current at dipole j on the potential recorded at electrode i . ϵ is an $M \times 1$ vector of additive noise. M is typically much smaller than N , making the problem ill-posed.

$$\mathbf{d} = \mathbf{L}\mathbf{j} + \epsilon \quad (1)$$

The source localization problem is then to recover \mathbf{j} based on the measurements and the estimate of \mathbf{L} . Various algorithms have been proposed to solve this problem, corresponding to different ways to choose one of the infinite number of solutions based on *a priori* criteria of what properties the solution should have. Reviews are available for example in [30], [31]. In all cases, the solution is dependent on \mathbf{L} , so an essential component for any of these methods is to have an accurate leadfield.

In EEG source localization, the leadfield is constructed based on a finite-element or boundary-element model of the head, which can incorporate patient-specific detail obtained for example via MRI [31]. In the peripheral nerve case, a finite-element model would be required because of the anisotropic conductivity of the nerve [23]. Due to the difficulty of obtaining appropriate nerve models, the method investigated here is founded on the desire to eliminate the need for a model entirely. Nonetheless, in order to solve the inverse problem, we still require some way of obtaining a forward problem solution. In the absence of a model, we rely instead on a collection of experimentally-obtained measurements. Because it is not feasible to experimentally isolate each possible location of a dipolar source in the nerve, we focus instead

on whole fascicles. The trade-off for eliminating the need for a model is therefore to impose a stricter limitation on the resolution. The task becomes one of pathway discrimination, rather than geometric localization. Note that the method does not assume that each stimulated pathway is an anatomically distinct fascicle, only that the activity of each pathway is located at a different position in the cross-section of the nerve. Therefore, from here on we will use the term “pathway” rather than “fascicle”, even though in the case of the rat sciatic nerve the stimulation of each distal nerve results in the activation of a separate fascicle at the level of the recording cuff.

We will use the term “experimental leadfield” to refer to a collection of observed measurement vectors that is built using a training set and will be used to classify future observations. This leadfield is a matrix in which each column is a 56-element vector corresponding to the measurements obtained from the recording cuff at a given instant. The goal is to construct a set of such vectors that are sufficiently representative of the activity produced by each stimulated nerve to be able to correctly identify future recordings by solving the inverse problem. Each column in the leadfield constructed in this way thus corresponds to an instantaneous spatial pattern of activity produced by an entire stimulated pathway. Each pathway will be associated with several vectors, because different patterns of activity will be produced as a compound action potential (CAP) travels in that pathway along the length of the recording cuff. The goal of the proposed method is therefore to be able to reconstruct the activity inside the nerve at a particular time instant. In this way, if sufficiently good spatial discrimination can be achieved, it will be possible as a second step to reconstruct the time course of the activity. In the present study, however, we focus strictly on the spatial discrimination. Because each pathway is associated with multiple patterns, corresponding to different longitudinal positions of the CAP, the method does not assume that the geometry of the branches is constant along the length of the recording cuff.

The experimental leadfield is constructed using a training set that includes only observations of single-pathway activity, because the system should be able to identify combinations of fascicles based only on its knowledge of the single-pathway base cases. The process of constructing the experimental leadfield is as follows. The main steps are summarized in Figure 4.

- 1) *Removal of bad channels*: In each trial, if the signal from a channel of the recording cuff has excessive variance compared to the other channels (more than 4 standard deviations away from the mean of the variances among all channels) or very small amplitude (amplitude range less than 0.1% of the greatest range among all channels), it is marked as a bad channel, and not used in the discrimination task. This removal is performed before converting the remaining channels to a common average reference.
- 2) *Form training and testing sets*: The trials are divided into a training set and a testing set, for each of the seven possible combinations of pathways (using the acronyms T, P, and S for the cases where the tibial, peroneal, and sural nerves are stimulated, respectively, the seven

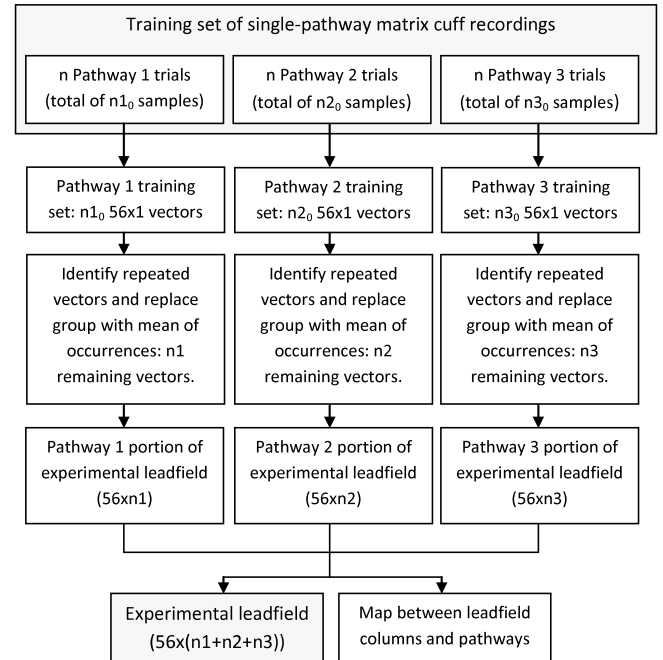


Fig. 4. Flowchart illustrating the main steps of the experimental leadfield construction process.

combinations are T, P, S, TP, TS, PS, and TPS). In the case of the multi-pathway combinations, all trials belong to the testing set. In each single-pathway case, the trials are divided into 5 groups, and the performance will be measured using 5-fold cross-validation. Accordingly, the multi-pathway performance will be evaluated 5 times, using a different training set each time but always the same testing set (i.e., all multi-pathway trials).

- 3) *Identify distinct patterns*: The training set of each single-pathway case is examined in order to identify the set of distinct measurement vectors that occur within it. Each new vector must be examined against all the previously seen vectors in order to determine whether it is a new pattern or one that has already been recorded. Ideally, each trial should produce exactly the same activity, so that a small number of patterns (corresponding to the different positions of the CAP along the recording cuff) should occur many times. In practice, this may not be the case, due to noise and the slight movement of the recording cuff.

For each trial, the measurement vectors used are from a time interval delimited by the peaks of the action potential recordings at the first and last contacts (excluding bad channels), plus 0.1 ms before and after this interval. A collection of vectors is built using these time instants from all the training set trials corresponding to a given stimulated nerve. From this collection of vectors we identify recurring patterns as follows.

- a) Each vector is normalized with respect to its entry with the largest absolute value.
- b) Each new vector is compared to all previously observed ones. A new vector v_2 is deemed to be

the same as an existing vector v_1 if the condition in Equation 2 holds true. The value of 0.3 was chosen empirically as a means to obtain meaningful groupings that allow for some variation in the instances of a given pattern, while still distinguishing patterns that genuinely reflect different sources of activity.

$$\|v_1 - v_2\|_2 < 0.3\|v_1\|_2 \quad (2)$$

c) If a vector has not been observed before, it is added to the set of distinct patterns. If the current vector corresponds to an already observed pattern then, for the purpose of future comparisons, each pattern is represented by the mean of all its occurrences.

4) *Eliminate unnecessary variables*: Once all vectors have been examined, any vector that occurred only once is deemed not to be useful for identifying future observations and therefore is removed, in order to produce a leadfield representing fewer, more meaningful variables.

5) *Form experimental leadfield*: The remaining vectors are gathered to form the columns of the experimental leadfield. The leadfield contains the vectors identified for all of the single-pathway cases, but we keep track of which columns correspond to which pathway.

4) *Identification of pathway combinations*: Once the leadfield has been constructed according to the procedure in the previous section, two situations can arise: the problem can be either underdetermined or overdetermined. The far more likely of the two, and the one dealt with here, is that of an underdetermined problem: the number of measurements is much smaller than the number of different patterns observed, so that the leadfield has more columns than rows. This is the same type of situation that typically arises when using a model-based leadfield. Many of the principles needed in that context to solve an ill-posed inverse problem can therefore be applied here as well, and algorithms borrowed from EEG source localization can still be used. Here, we use the common approach known as Tikhonov regularization [32], which balances two objective: minimizing the residual, and minimizing the norm of the solution, as expressed in Equation 3. The corresponding solution then takes the form shown in Equation 4.

$$\hat{\mathbf{j}} = \arg \min_{\mathbf{j}} \{ \|\mathbf{C}_\epsilon^{-0.5}(\mathbf{L}\mathbf{j} - \mathbf{d})\|^2 + \lambda \|\mathbf{H}\mathbf{j}\|^2 \} \quad (3)$$

$$\hat{\mathbf{j}} = (\mathbf{H}^t\mathbf{H})^{-1}\mathbf{L}^t[\mathbf{L}(\mathbf{H}^t\mathbf{H})^{-1}\mathbf{L}^t + \lambda\mathbf{C}_\epsilon]^{-1}\mathbf{d} \quad (4)$$

\mathbf{d} and \mathbf{L} are as described in Equation 1. $\hat{\mathbf{j}}$ is the vector of estimated source activations, each ‘‘source’’ in this case corresponding to a given spatial pattern of potentials obtained from the training set. \mathbf{C}_ϵ is the $M \times M$ noise covariance matrix, here assumed to be the identity matrix. λ is the regularization parameter, which is used to balance the accuracy of the estimate and the simplicity of the solution. This parameter is chosen using the L-curve method [33], which relies on finding the ‘‘corner’’ on a plot of the norm of the residual versus the norm of the solution. Lastly, \mathbf{H} is an $N \times N$ matrix used to

assign different weights to the variables. Here, we use the weighted minimum-norm method (WMN) [30], in which \mathbf{H} simply compensates for the different norms of the leadfield columns, as shown in Equation 5.

$$\begin{cases} H_{ii} = L_{1..M,i}^T L_{1..M,i} \\ H_{ij} = 0, i \neq j \end{cases} \quad (5)$$

The appeal of WMN in this situation stems from its lack of geometrical assumptions. Several source localization algorithms rely on the fact that each variable corresponds to a location in space, and that the activity at nearby locations is likely to be related [34], whereas in our case the variables do not have this kind of geometrical relationships. It is also apparent that a typical solution should consist of only a small number of non-zero variables. Indeed, a CAP in a given pathway should ideally correspond to a single column of the experimental leadfield. Even considering a complex source distribution involving several active pathways, the total number of variable will still be fairly small. Accordingly, it is reasonable to choose an inverse problem method that produces sparse solutions. We choose for this purpose to use FOCUSS [35], using as the initial estimate the WMN estimate. FOCUSS is an iterative application of the WMN method, where the weight matrix \mathbf{H} at each step is a diagonal matrix whose entries are based on the source estimates from the previous iteration. In this way, locations that were found to have significant activity in one iteration are favoured in the next iteration. As the number of iterations increases, the activity becomes concentrated in a small number of locations, and tends to zero elsewhere. The process stops when the solution is no longer changing significantly from one iteration to the next, or if the number of nonzero elements in the solution starts to increase. Like WMN, we regularize the FOCUSS algorithm using Tikhonov regularization and the L-curve method.

5) *Evaluation of the results*: The columns of the experimental leadfield correspond to instantaneous patterns of activity. Therefore, the pathway discrimination task is carried out at each time instant by solving the inverse problem. However, to summarize the performance of the method, it is beneficial to develop a more concise metric reflecting the activity over the course of an entire trial. For this purpose, a set of three values between 0 and 1 was computed, termed ‘‘activation indices’’, describing the relative estimated activations of the three pathways during an entire trial. In what follows, the estimate vector for a given time instant is denoted \mathbf{j}_t , the set of variables corresponding to pathway i is denoted s_i and is of size n_i , there are n_t time instants in a given trial, and the 3×1 vector of activation indices is denoted A . A_0 denotes a non-normalized version of A used as an intermediate step in the computations. The activation indices are then computed as shown in Equations 6 through 8.

$$\left\{ \mathbf{J} | \mathbf{J}_{1 \dots (n_1+n_2+n_3), t} = \frac{\mathbf{j}_t}{\|\mathbf{j}_t\|_\infty} \right\} \quad (6)$$

$$A_{0i} = \frac{\sum_{k \in s_i} \left(\frac{\sum_{t=1}^{n_t} \mathbf{J}_{k,t}}{n_t} \right)}{n_i} \quad (7)$$

$$A = \left| \frac{A_0}{\|A_0\|_\infty} \right| \quad (8)$$

III. RESULTS

When the experimental leadfield process described in the Methods section was applied to the sciatic nerve recordings, the number of columns in the 25 resulting leadfields (5-fold cross-validation in each of 5 rats) ranged from 176 to 384.

Figure 5 shows the mean of the three activity estimates for each pathway combination and each rat. These means are taken on the agglomeration of the results in all 5 testing sets. The figure reveals that in the single-pathway cases the algorithm was successful in identifying the stimulated pathway as by far the most active. Activity estimates of the other pathways were in most cases small, but not insignificant. As for the multi-pathway cases, the algorithm was less successful in identifying the active pathways. Although a few cases were close to being accurate (e.g. Rat 1, tibial + peroneal and tibial + sural), inactive pathway activities estimates were still high, and on the whole the method was not reliable.

Figure 5 gives a useful overview of the algorithm's ability to assess the activity of the different pathways. It would also be useful to know how often the algorithm can correctly identify the exact combination of active pathways. In order to measure this aspect of the performance, the activity estimates computed above were thresholded at 0.2. A pathway is deemed active if it is above this threshold, and inactive otherwise. We then computed the percentage of trials in which the combination of active pathways is exactly accurate, for each pathway combination and rat. The success rates were averaged across the 5 testing sets, and the results are shown in Figure 6.

Figure 6 is in accordance with Figure 5 in showing that the algorithm was more successful at correctly identifying single-pathway cases than multiple-pathway ones. The mean success rate over the 15 single-pathway cases was 68.5%, with a minimum of 19.4% and a maximum of 95%. On the other hand, the mean success rate over the 20 multiple-pathway cases was 25.3%, with a minimum of 1.3% and a maximum of 54.6%. Note that by consulting Figure 5, we can see that single-pathway cases with low performance in Figure 6 were likely due to inactive pathway erroneously being identified as active, rather than the correct active pathway being missed. The proportions of false positives and false negatives of course depends on the threshold that we use. The use of 0.2 was an attempt to balance the need of the single- and multi-pathway cases. If we focus only on single-pathway cases, it is clear from Figure 5 that the number of false positives in the single-pathway cases could be reduced by raising the threshold. In that case, we can simply select the pathway with the highest activation, which is equivalent to setting the threshold to 1, since the activation indices are normalized to the highest of the three values. This is illustrated in the second set of bars in Figure 6, which is obtained in the same way as first set of bars except with the threshold set to 1 instead of 0.2. This change of threshold raises the mean success rate of the single-pathway cases to 94.2%, and lowers that of the multiple-pathway cases to 0%. The complete relationship between the multi-pathway and single-pathway success rates as the threshold varies in

shown in Figure 7. As indicated on the figure, our initial threshold choice of 0.2 corresponds to the corner of the curve.

IV. DISCUSSION

We investigated a novel approach for pathway discrimination in peripheral nerves, inspired by bioelectric source localization but designed to avoid that method's sensitivity to its model-based forward problem solution. Rather than solve the forward problem using a finite-element model, we built an experimental leadfield using recordings corresponding to each of the single-pathway cases of interest. Our goal was then to use this leadfield to identify active pathways in both single- and multi-pathway previously unseen cases. The approach was evaluated on 56-channel recordings from a 1 mm-diameter spiral cuff placed on a rat sciatic nerve. The reader should keep in mind that the geometry of the cuff, the size of the nerve and the layout of the fascicles may all have an impact on the success of the pathway discrimination.

A. Technical issues

The intended stimulation parameters consisted of 10 μ s 2 mA pulses, 2 mA being comfortably higher than the thresholds reported in the literature for pulses of this duration [15], [36]–[38]. In practice, however, the parameters were somewhat different due to technical difficulties with the stimulators, leading to the values described in the Methods section. As the pulses were still able to produce CAPs, this issue has very limited impact on our results. Indeed, knowledge of the specific fiber recruitment obtained is not crucial to our study as long as it is consistent between trials, because all that is required is that the fascicles produce distinct spatial patterns. The second issue was that the large number of channels of the recording cuff created the need for a large and heavy connector that had to be held in place manually in several experiments, such that there may have been some slight movement of the recording cuff over the course of a given experiment. Although both the cuff movement and the presence of a stimulation artefact affect the quality of the recordings, similar issues are to be expected *in vivo*, in the form of slight changes in cuff position during limb movements and the presence of nearby bioelectric sources such as EMG. Therefore, although the experimental issues that we encountered may have affected our results quantitatively, they do not invalidate any of our qualitative conclusions regarding the performance of an experimental leadfield in practice.

B. Advantages and disadvantages of an experimental leadfield compared to a model-based leadfield

An important advantage of the experimental leadfield is that the number of variables to solve for in the inverse problem is much smaller than in the model-based approach. In the present study, the number of columns in the experimental leadfields shows that there was variability in the measurements: given the 20 kHz sampling rate, the 23 mm length of the recording cuff, and the conduction velocities of large fibers (36 to 120 m/s [39]), a CAP dominated by large fiber activity would take approximately 4 to 13 time samples to propagate through the

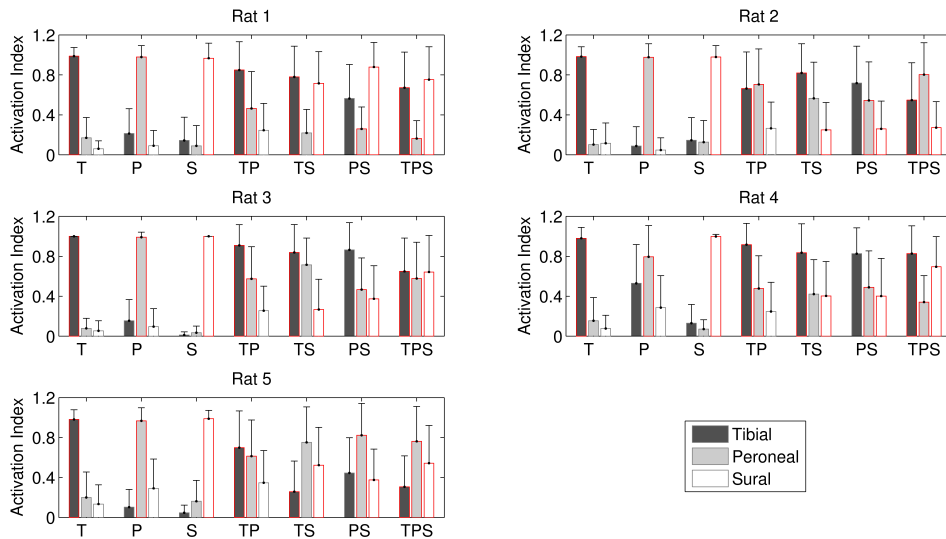


Fig. 5. Means of the activity indices for the three pathways, for each rat and pathway combination. The abbreviations are as follows: Tibial (T), Peroneal (P), Sural (S), Tibial and Peroneal (TP), Tibial and Sural (TS), Peroneal and Sural (PS), and Tibial, Peroneal, and Sural (TPS). In each case, the nerves being stimulated are outlined in red.

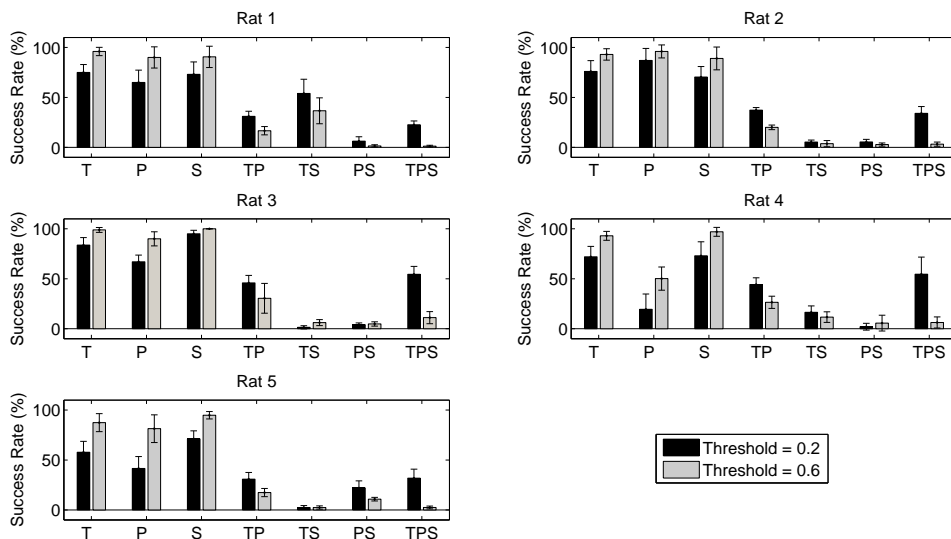


Fig. 6. Success rate for identifying the exact combination of active pathways, for each rat and pathway combination. The standard deviation is based on the 5 repetitions of the cross-validation process. The abbreviations are the same as in Figure 5. The threshold for a pathway to be considered active is 0.2 in the first set of bars, and 1 in the second set of bars.

cuff. In the ideal situation, therefore, the three pathways would result in fewer than 40 columns in the experimental leadfield (creating an overdetermined problem and calling for different methods to solve it), whereas in practice the value ranged between 176 and 384 as a result of the variations between trials. On the other hand, these numbers of variables were in all cases much smaller than what would be needed using a model-based distributed linear approach (corresponding to the algorithms described in Section II-A4), where the number of variables could be on the order of thousands to tens of thousands depending on the level of detail of the finite element

model and how fine a mesh is used.

Another crucial difference between the experimental and model-based leadfield approaches is the spatial resolution being sought. The experimental leadfield was presented here as limited in resolution to whole fascicles. Although this is accurate in the context of this study, in the more general case the limit is actually determined by the pathways that can be isolated experimentally and individually activated, either through direct stimulation or through indirect means such as cutaneous stimulation or passive limb motion. The pathways encoded in the experimental leadfield could therefore, de-

pending on the situation, be whole fascicles, sub-fascicular groups of axons, or functional groups of several fascicles. Because of this need for experimental activation of specific locations, the method is better suited to the peripheral nerve case than to EEG/MEG or ECG localization, where accessing specific regions individually is much more difficult. In the case of recent studies that use leadfields obtained using coarse models to identify fascicles [26], it is unclear what level of performance would be obtained if finer resolution was required. An experimental leadfield approach, on the other hand, could possibly overcome this issue if small pathways can be isolated experimentally. On a related note, the results presented here are based on compound action potential (CAP) recordings. The signal-to-noise ratio is therefore higher than what would be obtained during most natural activity (e.g. [19], [20]), which was helpful in assessing the methods but is less realistic. The choice of stimulated rather than natural neural activity in this study was motivated by the need to be able to simultaneously activate the pathways in any combination. If using the experimental leadfield in practice, it would be advisable to base the training set on the natural activity of different pathways, rather than direct stimulation. In this way, the training set will be more closely related to the activity that will be observed in practice.

Of course, the need to collect sample recordings for each pathway of interest is a practical disadvantage of the experimental leadfield approach compared to a model-based approach, but given a sufficient improvement in performance, this drawback does not seem insurmountable. Additionally, a model-based leadfield's advantage in this respect is only significant if no nerve-specific calibration of the model is required.

C. Outlook

The success of the experimental leadfield method in the single-pathway cases confirms the findings in the literature [14]–[17], [19], [20] that nerve cuff recordings can in fact contain sufficient information to discriminate the activity of different pathways, despite the fact that they increase the uniformity of the electric field around the nerve [40], [41]. None of these previously reported studies, however, have provided any suggestion of how the methods could be extended to the identification of multiple simultaneously active pathways. Source localization techniques provide a methodology for reconstructing distributions with multiple sources, as well as to deal with uncertainty in the measurements, and so have been investigated recently [23], [25]–[27]. Nonetheless, this type of method is vulnerable to modeling errors that will result in inaccurate forward problem solutions. The methodology proposed here retains the advantages of the inverse problem framework of bioelectric source localization, while removing the dependency on accurate modeling.

The limited performance in the multi-pathway cases of our study is primarily a reflection of the underdetermined nature of the problem, coupled with the uncertainty in the measurements. As the source configuration becomes more complex, reconstruction becomes more difficult, and noise

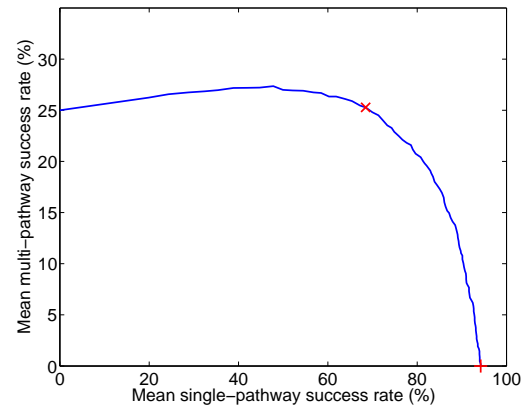


Fig. 7. Relationship between the mean success rates of the multi-pathway and single-pathway cases as the threshold for considering a pathway active is varied. The markers indicate the thresholds used in Figure 6: 0.2 (×) and 1 (+).

becomes a greater obstacle. As a result, sources of error that were minor enough for the single-pathway cases to be successful can become more significant in multi-pathway cases and prevent us from achieving successful discrimination. The nature of these difficulties suggests several avenues by which performance could be improved. First, more effective regularization approaches tailored to this novel inverse problem should be sought. In particular, the addition of temporal information should be investigated, by taking into account the fact that the spatial patterns (i.e., experimental leadfield columns) produced as a CAP travels along a pathway should occur in a specific order. Temporal coupling between consecutive instants could therefore be used to improve performance and ensure that the resulting solution is physiologically plausible. In addition, the influence on performance of the cuff geometry, number of recording contacts, and the number and location of the fascicles within the nerve are complex issues that will require more study, both to improve multi-pathway performance and to make the transition from stimulated to natural nerve activity. The experimental leadfield approach provides a method by which the influences of these different factors can be investigated. In other words, a key contribution of this paper is to provide the first viable framework for the study of multi-pathway selective nerve cuff recordings.

ACKNOWLEDGMENT

The authors would like to thank Lori Dixon, Ashlie Soko and Dr. Dimitry Sayenko for their invaluable help with the experiments.

REFERENCES

- [1] M. Hansen, M. K. Haugland, and T. Sinkjaer, "Evaluating robustness of gait event detection based on machine learning and natural sensors," *IEEE Trans. Neural Sys. Rehab. Eng.*, vol. 12, no. 1, pp. 81–88, Mar 2004.
- [2] A. Inmann and M. Haugland, "Functional evaluation of natural sensory feedback incorporated in a hand grasp neuroprosthesis," *Med. Eng. Phys.*, vol. 26, no. 6, pp. 439–447, Jul 2004.

- [3] G. A. Kurstjens, A. Borau, A. Rodriguez, N. J. Rijkhoff, and T. Sinkjaer, "Intraoperative recording of electroneurographic signals from cuff electrodes on extradural sacral roots in spinal cord injured patients," *J. Urology*, vol. 174, no. 4 Pt 1, pp. 1482–1487, Oct 2005.
- [4] G. S. Dhillon, S. M. Lawrence, D. T. Hutchinson, and K. W. Horch, "Residual function in peripheral nerve stumps of amputees: implications for neural control of artificial limbs," *J. Hand Surg.*, vol. 29, no. 4, pp. 605–15; discussion 616–8, Jul 2004.
- [5] S. Micera, X. Navarro, J. Carpaneto, L. Citi, O. Tonet, P. M. Rossini, M. C. Carrozza, K. P. Hoffmann, M. Vivo, K. Yoshida, and P. Dario, "On the use of longitudinal intrafascicular peripheral interfaces for the control of cybernetic hand prostheses in amputees," *IEEE Trans. Neural Sys. Rehab. Eng.*, vol. 16, no. 5, pp. 453–472, Oct 2008.
- [6] S. M. Lawrence, G. S. Dhillon, and K. W. Horch, "Fabrication and characteristics of an implantable, polymer-based, intrafascicular electrode," *J. Neurosci. Meth.*, vol. 131, no. 1-2, pp. 9–26, Dec 30 2003.
- [7] S. M. Lawrence, G. S. Dhillon, W. Jensen, K. Yoshida, and K. W. Horch, "Acute peripheral nerve recording characteristics of polymer-based longitudinal intrafascicular electrodes," *IEEE Trans. Neural Sys. Rehab. Eng.*, vol. 12, no. 3, pp. 345–348, Sep 2004.
- [8] A. Branner, R. B. Stein, and R. A. Normann, "Selective stimulation of cat sciatic nerve using an array of varying-length microelectrodes," *J. Neurophys.*, vol. 85, no. 4, pp. 1585–1594, Apr 2001.
- [9] A. Branner, R. B. Stein, E. Fernandez, Y. Aoyagi, and R. A. Normann, "Long-term stimulation and recording with a penetrating microelectrode array in cat sciatic nerve," *IEEE Trans. Biomed. Eng.*, vol. 51, no. 1, pp. 146–157, Jan 2004.
- [10] J. Taylor, N. Donaldson, and J. Winter, "Multiple-electrode nerve cuffs for low-velocity and velocity-selective neural recording," *Med. Biol. Eng. Comput.*, vol. 42, no. 5, pp. 634–643, Sep 2004.
- [11] R. Rieger, J. Taylor, E. Comi, N. Donaldson, M. Russold, C. M. Mahony, J. A. McLaughlin, E. McAdams, A. Demosthenous, and J. C. Jarvis, "Experimental determination of compound action potential direction and propagation velocity from multi-electrode nerve cuffs," *Med. Eng. Phys.*, vol. 26, no. 6, pp. 531–534, Jul 2004.
- [12] R. Rieger, M. Schuettler, D. Pal, C. Clarke, P. Langlois, J. Taylor, and N. Donaldson, "Very low-noise ENG amplifier system using CMOS technology," *IEEE Trans. Neural Sys. Rehab. Eng.*, vol. 14, no. 4, pp. 427–437, Dec 2006.
- [13] B. K. Lichtenberg and C. J. De Luca, "Distinguishability of functionally distinct evoked neuroelectric signals on the surface of a nerve," *IEEE Trans. Biomed. Eng.*, vol. 26, no. 4, pp. 228–237, Apr 1979.
- [14] J. J. Struijk, M. K. Haugland, and M. Thomsen, "Fascicle selective recording with a nerve cuff electrode," in *Proc. 18th Ann. Int. Conf. IEEE EMBS*, Amsterdam, 31 Oct-3 Nov 1996, pp. 361–362.
- [15] M. Sahin and D. M. Durand, "Selective recording with a multi-contact nerve cuff electrode," in *Proc. 18th Ann. Int. Conf. IEEE EMBS*, Amsterdam, Netherlands, 1996, pp. 369–370.
- [16] P. R. Christensen, Y. Chen, K. D. Strange, K. Yoshida, and J. A. Hoffer, "Multi-channel recordings from peripheral nerves: 4. Evaluation of selectivity using mechanical stimulation of individual digits," in *Proc. 2nd Ann. Conf. IFESS*, Burnaby, BC, Canada, 1997.
- [17] P. B. Yoo and D. M. Durand, "Selective recording of the canine hypoglossal nerve using a multicontact flat interface nerve electrode," *IEEE Trans. Biomed. Eng.*, vol. 52, no. 8, pp. 1461–1469, Aug 2005.
- [18] W. Tesfayesus and D. M. Durand, "Blind source separation of peripheral nerve recordings," *J. Neural Eng.*, vol. 4, no. 3, pp. S157–67, Sep 2007.
- [19] H. S. Cheng, M. S. Ju, and C. C. Lin, "Estimation of peroneal and tibial afferent activity from a multichannel cuff placed on the sciatic nerve," *Muscle Nerve*, vol. 32, no. 5, pp. 589–599, Nov 2005.
- [20] J. Rozman, B. Zorko, and M. Bunc, "Selective recording of electroneurograms from the sciatic nerve of a dog with multi-electrode spiral cuffs," *Jpn. J. Physiol.*, vol. 50, no. 5, pp. 509–514, Oct 2000.
- [21] T. Stieglitz, M. Schuettler, and K. P. Koch, "Implantable biomedical microsystems for neural prostheses," *IEEE Eng. Med. Biol. Mag.*, vol. 24, no. 5, pp. 58–65, Sep-Oct 2005.
- [22] J. Zariffa and M. R. Popovic, "Application of EEG source localization algorithms to the monitoring of active pathways in peripheral nerves," in *Proc. IEEE EMBS 30th Ann Int Conf.*, Vancouver, BC, Canada, August 21-24 2008, pp. 4216–4219.
- [23] —, "Localization of active pathways in peripheral nerves: A simulation study," *IEEE Trans. Neural Sys. Rehab. Eng.*, vol. 17, no. 1, pp. 53–62, 2009.
- [24] M. Schuettler, I. F. Triantis, B. Rubehn, and T. Stieglitz, "Matrix cuff electrodes for fibre and fascicle selective peripheral nerve recording and stimulation," in *Proc. 12th Ann. Conf. IFESS*, Philadelphia, PA, 2007.
- [25] J. Zariffa, M. K. Nagai, Z. J. Daskalakis, and M. R. Popovic, "Bioelectric source localization in the rat sciatic nerve: Initial assessment using an idealized nerve model," in *In: Doessel, O., Schlegel, W.: IFMBE Proceedings 25/IX, World Congress on Medical Physics and Biomedical Engineering, Sept. 7-12, Munich, Germany, 2009*, pp. 138–141.
- [26] B. Wodlinger and D. M. Durand, "In vivo localization of fascicular activity," *Proc. 31st Ann. Int. Conf. IEEE EMBS*, vol. 1, pp. 2940–2942, 2009.
- [27] —, "Localization and recovery of peripheral neural sources with beamforming algorithms," *IEEE Trans. Neural Sys. Rehab. Eng.*, vol. 17, no. 5, pp. 461–468, Oct 2009.
- [28] J. U. Meyer, T. Stieglitz, O. Scholz, W. Haberer, and H. Buetel, "High density interconnects and flexible hybrid assemblies for active biomedical implants," *IEEE Trans. Adv. Packaging*, vol. 24, pp. 366–375, 2001.
- [29] H. Schmalbruch, "Fiber composition of the rat sciatic nerve," *Anat. Rec.*, vol. 215, no. 1, pp. 71–81, May 1986.
- [30] R. D. Pascual-Marqui, "Review of methods for solving the EEG inverse problem," *IJBEM*, vol. 1, no. 1, pp. 75–86, 1999.
- [31] C. M. Michel, M. M. Murray, G. Lantz, S. Gonzalez, L. Spinelli, and R. Grave de Peralta, "EEG source imaging," *Clin. Neurophysiol.*, vol. 115, no. 10, pp. 2195–2222, Oct 2004.
- [32] A. N. Tikhonov and V. Y. Arsenin, *Solutions of ill-posed problems*. Washington; New York: Winston; distributed solely by Halsted Press, 1977.
- [33] P. C. Hansen, "Analysis of discrete ill-posed problems by means of the L-curve," *SIAM Rev.*, vol. 34, pp. 561–580, 1992.
- [34] R. D. Pascual-Marqui, "Standardized low-resolution brain electromagnetic tomography (sLORETA): technical details," *Methods Find. Exp. Clin. Pharmacol.*, vol. 24 Suppl D, pp. 5–12, 2002.
- [35] I. F. Gorodnitsky, J. S. George, and B. D. Rao, "Neuromagnetic source imaging with FOCUSS: a recursive weighted minimum norm algorithm," *Electroencephalogr. Clin. Neurophysiol.*, vol. 95, no. 4, pp. 231–251, Oct 1995.
- [36] X. Navarro, E. Valderrama, T. Stieglitz, and M. Schuettler, "Selective fascicular stimulation of the rat sciatic nerve with multipolar polyimide cuff electrodes," *Restor. Neurol. Neurosci.*, vol. 18, pp. 9–21, 2001.
- [37] W. M. Grill and J. T. Mortimer, "Quantification of recruitment properties of multiple contact cuff electrodes," *IEEE Trans. Neural Sys. Rehab. Eng.*, vol. 4, no. 2, pp. 49–62, Jun 1996.
- [38] D. J. Tyler and D. M. Durand, "Functionally selective peripheral nerve stimulation with a flat interface nerve electrode," *IEEE Trans. Neural Syst. Rehabil. Eng.*, vol. 10, no. 4, pp. 294–303, Dec 2002.
- [39] E. R. Kandel and J. H. Schwartz, *Principles of neural science*. New York: McGraw-Hill, 2000.
- [40] J. J. Struijk, "The extracellular potential of a myelinated nerve fiber in an unbounded medium and in nerve cuff models," *Biophys. J.*, vol. 72, no. 6, pp. 2457–2469, Jun 1997.
- [41] J. H. Meier, W. L. C. Rutten, and H. B. K. Boom, "Extracellular potentials from active myelinated fibers inside insulated and noninsulated peripheral nerve," *IEEE Trans. Biomed. Eng.*, vol. 45, no. 9, pp. 1146–1154, 1998.